Molecular Catalysis 572 (2025) 114750

Contents lists available at ScienceDirect

Molecular Catalysis

journal homepage: www.journals.elsevier.com/molecular-catalysis

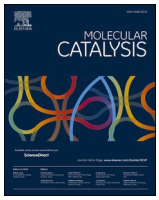

High surface area perovskite materials as functional catalyst supports for glycerol oxidation

Hamza S. Rabiu [a,b], James S. Hayward [a], Jonathan K. Bartley [a,*]

[a] Cardiff Catalysis Institute, School of Chemistry, Cardiff University, Cardiff, CF10 3AT, UK
[b] Present address: Department of Pure and Industrial Chemistry, Bayero University, 700241 Kano, Kano State, Nigeria

ARTICLE INFO

Keywords:
Perovskite supported catalysts
Glycerol oxidation
Lactic acid production
Glyceric acid production
Tartronic acid production

ABSTRACT

A series lanthanum perovskite supports ($LaBO_3$, where B = Cr, Mn, Fe, Co and Ni) were synthesised using a hard templating methodology with a mesoporous silica template (SBA-15). This methodology produced high surface area perovskites with surface areas of 70–160 $m^2\ g^{-1}$. 1 wt% AuPt was added to the perovskite supports using sol immobilisation and the resultant catalysts tested for the oxidation of glycerol. When the AuPt/$LaBO_3$ catalysts were tested for glycerol oxidation the product distributions *via* either the oxidation mechanism or a dehydration mechanism could be tuned by substituting different transition metals into the B site. In line with previous studies, AuPt/$LaMnO_3$ and AuPt/$LaCoO_3$ gave the highest yield of oxidation products (glyceric acid with small amounts of tartronic acid), AuPt/$LaCrO_3$ gave the highest yield of lactic acid through the dehydration pathway, while AuPt/$LaNiO_3$ and AuPt/$LaFeO_3$ gave a mixture of products from both the oxidation and dehydration pathways. The product distributions were found to change over the course of the reaction due to the relative rates of the two reaction pathways. For all catalysts except AuPt/$LaMnO_3$ the yield of oxidation products stopped after two hours, while all catalysts except AuPt/$LaMnO_3$ continued to produce lactic acid over the whole reaction. This suggests the perovskite supported catalysts are not stable over the course of the reaction. The most interesting behaviour was found for the AuPt/$LaFeO_3$ catalyst that gave a high initial selectivity to tartronic acid, although further studies are needed to elucidate the mechanism fully.

1. Introduction

Glycerol (GLY) is a versatile multifunctional organic molecule which is produced as a by-product from the transesterification of triacylglycerols to biodiesel [1–3]. Each carbon atom in the structure is bound to a hydroxyl group which gives it great potential for exploitation as a platform chemical. For this reason, the selective oxidation of glycerol over heterogeneous catalysts (commonly supported platinum group metals) has long been a subject of scientific interest [4]. It has been determined that the choice of catalyst [5], the size of the platinum group metal (PGM) [6] and the reaction conditions [7] can all significantly influence the selectivity and the rate of the reaction.

Scheme 1 shows the large distribution of products which can be formed from the oxidation of glycerol. Using heterogeneous catalysts for glycerol oxidation allows for an additional avenue to control reaction selectivity. The pioneering work of Prati *et al.* demonstrated that supported Au catalysts were active for the selective oxidation of glycerol [10]. It was found that Au/C could selectively produce glyceric acid through the sequential oxidation of glycerol. Further development of the Au catalysts found that the activity of the catalysts could be significantly increased through the addition of Pd [11,12] or Pt [11]. The most desirable products that can be produced from glycerol oxidation are either the C_3 oxidation products, glyceric acid (GA) and the sequential oxidation of this product, tartronic acid (TA); or lactic acid (LA) produced through the opposing dehydration pathway. To achieve the selective formation of these products, C-C scission must be hindered as much as possible. It is believed that this unfavourable cleavage leading to shorter carbon chnage molecules is as a result of the in-situ production of H_2O_2 from the reduction of O_2 by H_2O on the catalysts surface [13–15]. The application of hydrophobic materials as supports for the PGM has been shown to reduce this unfavourable C-C bond cleavage [16].

It has been well documented that the catalyst support has an influence on the conversion of glycerol and product selectivity under oxidative and basic conditions [17–19]. Single metal oxides and carbon are popular supports for glycerol oxidation, with carbon shown to be

* Corresponding author.
E-mail address: BartleyJK@cardiff.ac.uk (J.K. Bartley).

https://doi.org/10.1016/j.mcat.2024.114750
Received 14 October 2024; Received in revised form 22 November 2024; Accepted 28 November 2024
Available online 6 December 2024

more active than supports such as TiO_2 and Fe_2O_3 [11].

Supports such as Al_2O_3 and NiO are highly active, but have a large product distribution and are not very selective [20]. A study by Villa *et al.* [21] demonstrated the role of acid and basic sites on supports used for glycerol oxidation. It was found that basic sites contributed to a higher activity with a poor selectivity breakdown of products, and supports containing acid sites had a lower activity, but higher selectivity to glyceraldehyde and dihydroxyacetone, therefore, controlling this step allows for a greater product selectivity. This clearly demonstrates that the support has a significant role on the activity and selectivity to products, and therefore, tailoring a support with the desired characteristics to enhance a selected mechanistic pathway is the key to selective formation of a desired product.

Perovskite materials are potentially ideal candidates as support materials as they have high compositional flexibility (they can be synthesised using around 90 % of the metallic elements in the periodic table) allowing different metal cations to be present in the structural and surface lattice. This structural flexibility enables the introduction of the desired active sites, achieving site isolation through the intrinsic structure of the materials. Perovskites have the general formula ABO_3 where the larger A cation is typically a lanthanide, alkaline or alkaline-earth cation and the smaller B cation is a transition metal. Partial substitutions of the A and B sites are also possible which allows tailoring and tuning of their physiochemical properties.

However, perovskites are rarely used as catalyst supports due to the fact that high calcination temperatures are required to obtained a pure perovskite phase and this directly affects their surface area [22–24]. To achieve a good metal dispersion, a support material with surface area above 50 m^2/g is desired [25]. Efforts have been made to synthesize perovskite oxides using different methods to improve their surface area and mitigate the poor phase purity for them to be used as catalyst supports for metal nanoparticles [25,26]. Hutchings and coworkers have reported the use of supercritical anti-solvent precipitation for the synthesis of lanthanum-based perovskite oxides to improve the low surface area reported for convention methods [25]. Although the surface area is considerably improved by this method (achieving ca. 50 $m^2\ g^{-1)}$, the cost associated with recycling high pressure CO_2 and the phase purity of the perovskites produced are major drawbacks to the process.

Here we describe the use of hard templating with SBA-15 to synthesise high surface area lanthanum-based perovskites. The materials were investigated as supports for AuPt glycerol oxidation catalysts with the aim of tuning the reaction pathways to either lactic acid, glyceric acid or tatronic acid.

2. Experimental

Perovskite synthesis

The perovskite oxides ($LaBO_3$, where B = Cr, Mn, Fe, Co and Ni) were used as catalyst supports for the metal nanoparticles and synthesised by a hard templating method using SBA-15 as the template material.

Calculated amounts of $La(NO_3)_3{\cdot}6H_2O$ and $B(NO_3)_2{\cdot}nH_2O$, were dissolved in 10 ml of de-ionized water and added to a 10 ml citric acid solution (0.006 M) to give a total metal:citric acid ratio of 2:1. The mixture was added dropwise to a suspension of 1.0 g of SBA-15 in 10 ml de-ionized water and stirred for 2 h at room temperature. The solvent was evaporated at 80 °C for 24 h and the resultant solid ground to a fine powder before calcining at 500 °C for 2 h with a ramp rate of 2 °C min^{-1}. The impregnation of the precursor was repeated with a metal-citric acid ratio (1:1), followed by calcination at 700 °C for 2 h with a ramp rate of 2 °C min^{-1}. The resultant calcined material was washed with an aqueous solution of NaOH (2 M) to leach out the SBA-15 from the composite and then washed with de-ionized water at room temperature.

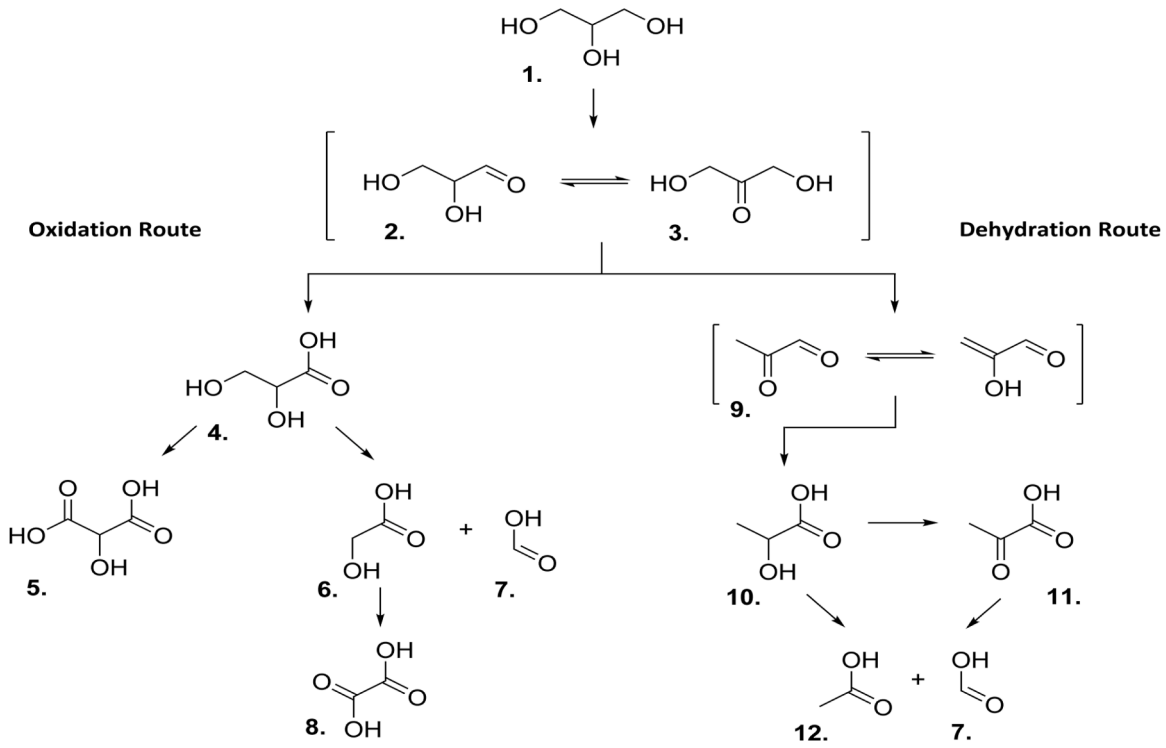

Scheme 1. The potential pathways and products from glycerol oxidation. Key: 1. Glycerol (GLY); 2. Glyceraldehyde (GLD); 3. Dihydroxyacetone (DHA); 4. Glyceric acid (GA); 5. Tartronic acid (TA); 6. Glycolic acid (GLA); 7. Formic acid (FA); 8. Oxalic acid (OA); 9. Pyruvaldehyde (PALD); 10. Lactic acid (LA); 11. Pyruvic acid (PA); 12. Acetic acid (AA) [8]. Reproduced under terms of the CC-BY license [9]. Copyright 2020, M. Douthwaite, N. Powell, A. Taylor, G. Ford, J.M. López, B. Solsona, N. Yang, O. Sanahuja-Parejo, Q. He, D.J. Morgan, T. Garcia, S.H. Taylor, published by Wiley-VCH.

Deposition of metals using sol immobilisation

An aqueous solution (400 mL) of $HAuCl_4$ (5 mg, 0.41 mL, 12.25 mg/ml) and H_2PtCl_6 (4.98 mg, 0.62 mL, 7.5 mg/ml) were prepared. Polyvinyl alcohol (PVA, 1 wt% aqueous solution, MW = 10 kDa) was freshly prepared and used as the stabilising agent. $NaBH_4$ (3.8 mL, 10 % aqueous solution) was also freshly prepared and used as the reducing agent. To an aqueous mixture of the $HAuCl_4$ and H_2PtCl_6 in a concentration to produce 1:1 ratio by mass, with 1 wt% of total metal in the prepared catalyst, the PVA solution was added (0.1 M, 1.3:1 PVA:metals ratio) with vigorous stirring for 2 min. $NaBH_4$ was subsequently added such that the $NaBH_4$:total metal ratio (mol/mol) was 6.5. The resulting solution was stirred for 30 min to allow the stabilisation of the reducing colloidal particles, followed by the addition of the perovskite material. The solution was left stirring for a further 1 h, followed by washing with distilled water and drying at 110 °C for 16 h.

Glycerol oxidation reactions

Glycerol oxidation experiments were carried out using a 50 ml Colaver reactor charged with an aqueous solution of glycerol (10 ml, 0.3 M) with a NaOH base (10 ml, 1.2 M) giving a glycerol:base ratio of 1:4. The catalyst was added to give a substrate:metal ratio of 1000:1. The reactor was heated to the reaction temperature using a silicone oil bath with a feedback loop to control the temperature. The round bottom flask was then sealed, purged 3 times with oxygen and pressurised to the required O_2 pressure. The oxygen inlet valve was opened to ensure oxygen pressure remains constant throughout the reaction. The reactor was then heated to temperature and the stirrer speed set to the desired speed (400 – 1000 rpm). Samples were taken at different time intervals and analysed by high performance liquid chromatography (HPLC) using UV and refractive index detectors. Reactants and products were separated using a Metacarb 67 H column. The eluent was an aqueous solution of phosphoric acid (0.01 M) at a flow rate of 0.25 ml min^{-1}. Each sample (0.5 ml) was diluted with eluent (4.5 ml) and products were identified by comparison with commercial samples. Quantification was achieved using an external calibration method, which allows an easy comparison between the HPLC sample response to that of target compounds.

Catalyst characterization

X-ray diffraction: Powder XRD patterns were obtained using a PANalytical X'pert Pro powder diffractometer with a Cu Kα source operated at 40 kV and 40 mA to obtain the data. Phase identification was performed using the X'Pert High Score utilising the ICDD database.

Nitrogen physisorption: Surface areas of the materials were determined using the BET method using a Quadrasorb surface area analyser. A 5-point analysis of each material was performed using 150 °C operating temperature with nitrogen as the adsorbate gas. Samples were degassed at the maximum temperature (250 °C) for 2 hours prior the analysis.

Thermal gravimetric analysis (TGA): Approximately 20 mg of the materials were analysed on a Seteram TGA/DTA in a flow of oxygen to acquire the decomposition mass losses of catalyst precursors as outlined in the catalyst support preparation section and to obtain suitable calcination temperatures to form pure phase support materials.

Transition electron microscopy (TEM): TEM analysis was carried out using a Jeol 2100 microscope equipped with a LAB6 filament operating at 200 kV. Each sample was prepared by dispersing the powder catalyst in ethanol and dropping the suspension onto a lacey carbon film on a 300-mesh copper grid. Particle size distributions were generated from a statistically relevant number of micrographs from which a total 100 particles were counted using imageJ software.

X-ray photoelectron spectroscopy (XPS): XPS measurements were performed using a Kratos Axis DLD photoelectron spectrometer equipped with a charge neutralizer and a Mg Kα X-ray source ($h\upsilon$ = 1253.6 eV) and monochromated Al Kα ($h\upsilon$ = 1486.6 eV). Using the Mg source, high resolution spectra were recorded with an analyser pass energy of 20 eV and 80 eV for survey scans while for the monochromated Al source an analyser pass energy of 40 eV for high resolution scans and 160 eV for survey scans were employed.

Microwave plasma atomic emission spectroscopy (MP-AES): MP-AES analysis was carried out using an Agilent 4100 instrument. The Au content was determined using the 242.795 nm and 267.595 nm emission lines and the Pt content was determined from the 265.945 nm and 270.240 nm emission lines.

Results and discussion

Catalyst characterisation

A series lanthanum containing perovskite oxide supports were synthesised, $LaBO_3$, containing different transition metal B sites (where B = Cr, Mn, Fe, Co and Ni). This was carried out by impregnating SBA-15 with solutions of metal nitrate salts and citric acid, followed by calcination and removal of the SBA-15 with base to give the perovskite materials. Thermogravimetric analysis was performed on the impregnated composite materials to determine the most appropriate calcination temperature to form the perovskite phase. The analysis was conducted from 30 °C to 900 °C, as typical temperatures required to form the perovskite phase are between 400 °C and 900 °C. The TGA results (Fig. 1) showed that there are consecutive weight losses in all the perovskite precursors with notable weight loss in each case beginning at around 400 °C. This can be attributed to decomposition of the metal nitrates and oxidation of the chelating agent (citric acid) present in the perovskite precursor [27].

The weight losses at higher temperature (≥700 °C) are attributed to the transition from single metal oxide phases to the perovskite oxide phase, with the transition temperature dependant on, and controlled by, the variable oxidation states of the transition metal in the B site of the perovskite oxides [28]. The chosen calcination temperature for the perovskite precursors was 700 °C, as the final weight loss event begins before this point for all the samples.

After calcination of the precursor at 700 °C the SBA-15 was removed using 2 M NaOH followed by a second calcination at 450 °C, and the XRD patterns of the resultant materials are shown in Fig. 2. The patterns of the calcined perovskites, except for $LaMnO_3$, all showed La_2O_3 was also present, and Fe_2O_3 was observed as a minor phase in $LaFeO_3$. The

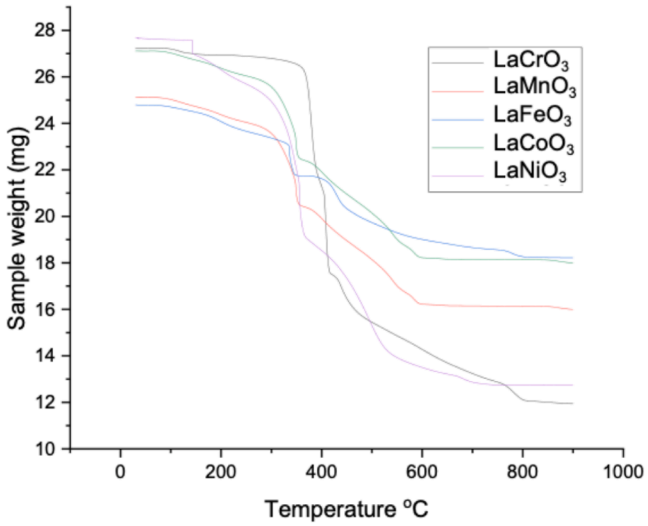

Fig. 1. TGA plot illustrating the weight loss from the $LaBO_3$-SBA-15 composites under calcination.

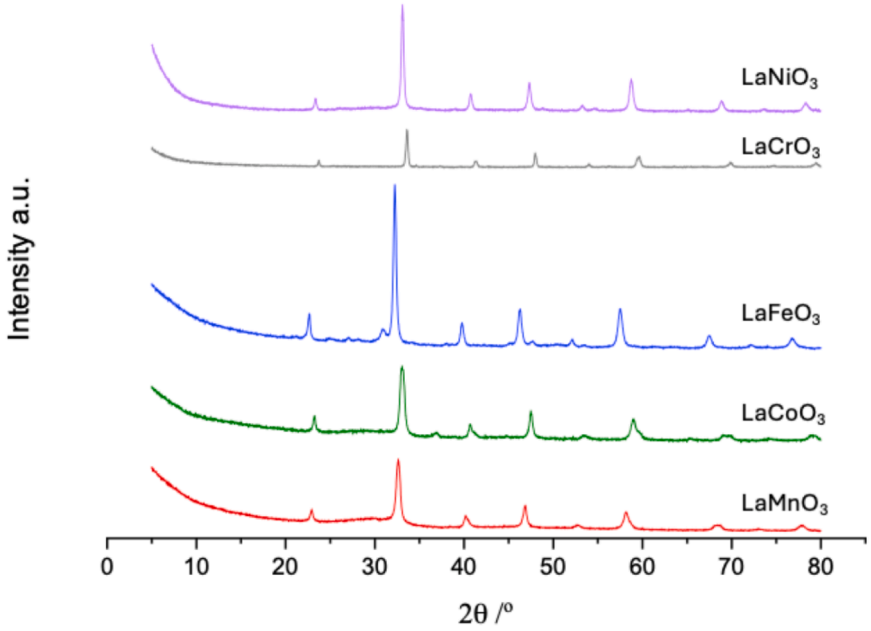

Fig. 2. Powder X-ray diffraction patterns of the $LaBO_3$ perovskite phases where the mixture rhombohedral, orthorhombic, and cubic phases are not differentiated).

semi quantitative ratio of the phases was calculated using the relative intensity ratios from the reference patterns and these are shown in Table 1, along with the crystallite sizes of the perovskite phases calculated using the Debye-Scherrer equation.

The observed impurity phases are proposed to be due to a non-stoichiometric recrystallisation of metal precursors in the SBA-15 pores resulting in a phase segregation of the metals coupled with a relatively low calcination temperature. The calcination temperature is known to have an influence on the formation of a single perovskite phase or phase segregated single oxides and we investigated this with the $LaCrO_3$ perovskite. High temperature is needed to form the perovskite and the single metal oxide phase content decreases with increasing temperature. However, the surface area is drastically reduced with increasing calcination temperature (Table S1) and so the temperature used is a compromise between retaining a high surface area and forming the desired perovskite phase (Figure S1 and Table S1). Table 2 shows the surface area of the materials at different stages of the synthesis process and it can be seen that the impregnated SBA-15 composites have a surface area of less than 500 $m^2\ g^{-1}$ compared to 750 $m^2\ g^{-1}$ for the starting SBA-15. This increases to around 600 $m^2\ g^{-1}$ on calcination, but then drops considerably when the SBA-15 template is removed. However, the surface areas of the synthesised supports of 70–125 $m^2\ g^{-1}$ are still very high compared to perovskites synthesised using other methods. Potentially the high surface area and small crystallite sizes of these supports will provide a larger distribution of defect sites on the surface of the perovskite materials, which allows the metals to coordinate to these defects and increases their stability when they are used in the liquid phase reaction. When 1 wt% of equal mass Au and Pt were added *via* sol immobilisation this surface area was retained.

Table 1
Phase composition calculated from ICDD relative intensity ratios of XRD patterns and crystallite sizes of the perovskite phases calculated using the Debye-Scherrer equation.

Catalyst Support	Phase Composition	Crystallite size (nm)
$LaMnO_3$	100 % $LaMnO_3$	7
$LaCoO_3$	96 % $LaCoO_3$ 4 % La_2O_3	3
$LaFeO_3$	86 % $LaFeO_3$ 12 % La_2O_3 2 % Fe_2O_3	12
$LaCrO_3$	89 % $LaCrO_3$ 11 % La_2O_3	5
$LaNiO_3$	91 % $LaNiO_3$ 9 % La_2O_3	3

Table 2
Surface areas of the perovskite based catalysts at different stages of the synthesis method.

Material	Surface Area ($m^2\ g^{-1}$)
SBA-15	756
$LaMnO_3$-SBA-15 Uncalcined	454
$LaMnO_3$-SBA-15 Calcined	587
$LaMnO_3$	95
1wt% AuPt/$LaMnO_3$	95
$LaCoO_3$-SBA-15 Uncalcined	488
$LaCoO_3$-SBA-15 Calcined	596
$LaCoO_3$	158
1wt% AuPt/$LaCoO_3$	158
$LaFeO_3$-SBA-15 Uncalcined	479
$LaFeO_3$-SBA-15 Calcined	562
$LaFeO_3$	68
1wt% AuPt/$LaFeO_3$	68
$LaCrO_3$-SBA-15 Uncalcined	471
$LaCrO_3$-SBA-15 Calcined	599
$LaCrO_3$	105
1wt% AuPt/$LaCrO_3$	105
$LaNiO_3$-SBA-15 Uncalcined	483
$LaNiO_3$-SBA-15 Calcined	599
$LaNiO_3$	125
1wt% AuPt/$LaNiO_3$	125

The metals were added to the support using a sol immobilization method that produces inherently small and well dispersed nanoparticles across the surface of the support. Bing able to achieve a consistent particle size distribution that is independent of the support material is crucial to decoupling the support properties from the metal nanoparticle catalysts and understanding the role of the perovskites in the reaction.

Transmission electron microscopy was conducted on each of the prepared supports with the images and particle size distribution (PSD) shown below (Figs. 3 and 4).

For all the perovskite supports the mean particle size was found to be approximately 2 nm with a standard deviation of around 1 nm. It appears that there is no strong correlation between particle size with either

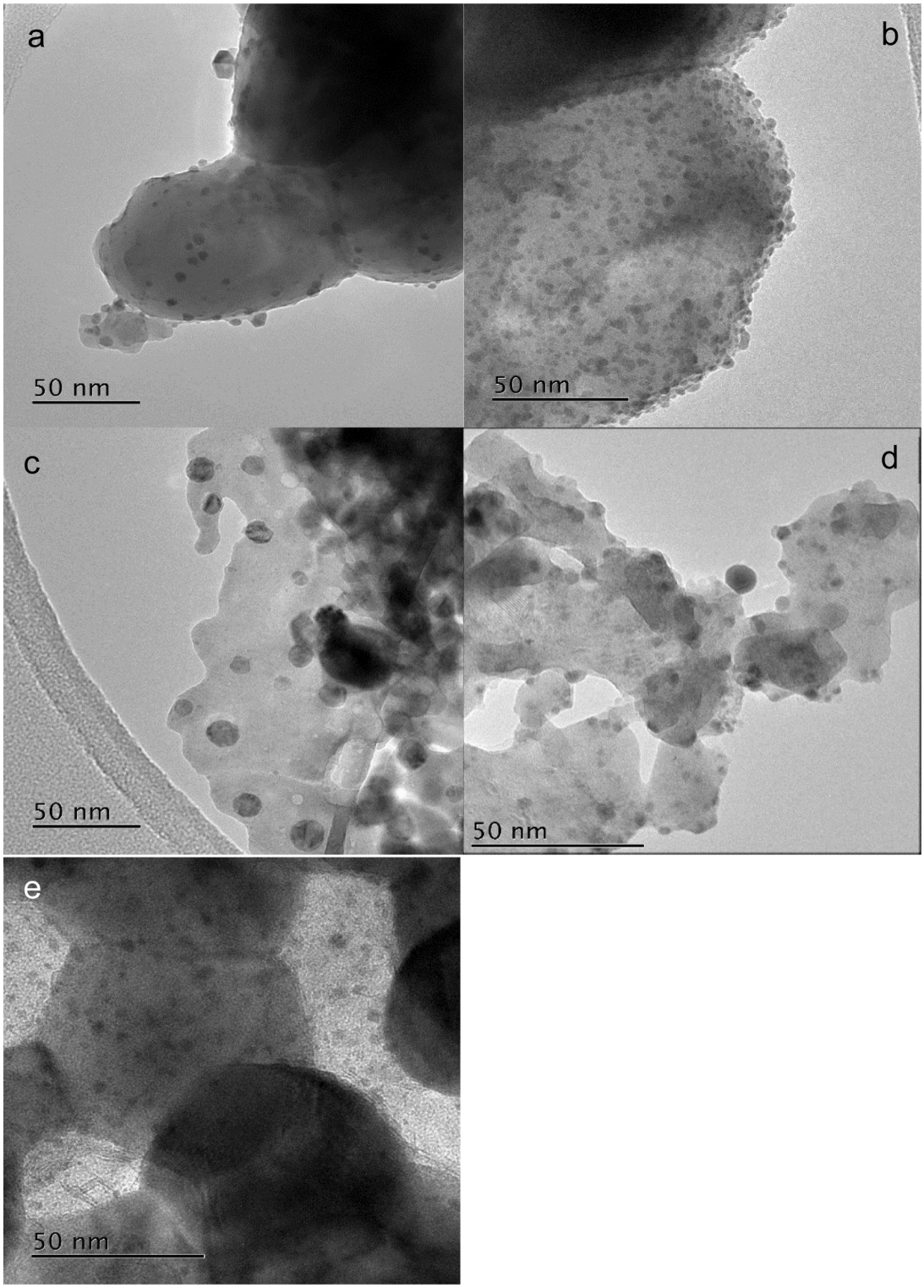

Fig. 3. Representative transmission electron micrographs of sol-immobilisation prepared AuPt supported on the various SBA-15 assisted $LaBO_3$ perovskite oxide supports. Where, (a) $LaCoO_3$, (b) $LaCrO_3$, (c) $LaFeO_3$, (d) $LaMnO_3$, and (e) $LaNiO_3$.

the relative surface area or the specific B site element used, confirming that the properties of the nanoparticles prepared using sol immobilisation are independent of the support material. It is likely that the small well-defined PSD observed for these catalysts is a result of its low metal loading [33]. These results confirm previous studies in literature which report that the conventional sol immobilisation technique generates small nanoparticles with well-defined PSD [8].

The catalysts were characterized by X-ray photoelectron spectroscopy (XPS) to provide insight into oxidation state of the metal nanoparticles and the relative Au-Pt surface composition and the Au and Pt 4f regions are shown in Figure S2. The Au peaks can be assigned to Au^0. Bulk Au^0 $4f_{7/2}$ peaks are typically observed at 84.0 eV with a doublet due to spin-orbit splitting of 3.7 eV, but supported nanoparticles show a shift in binding energies to lower energy when they are dispersed as

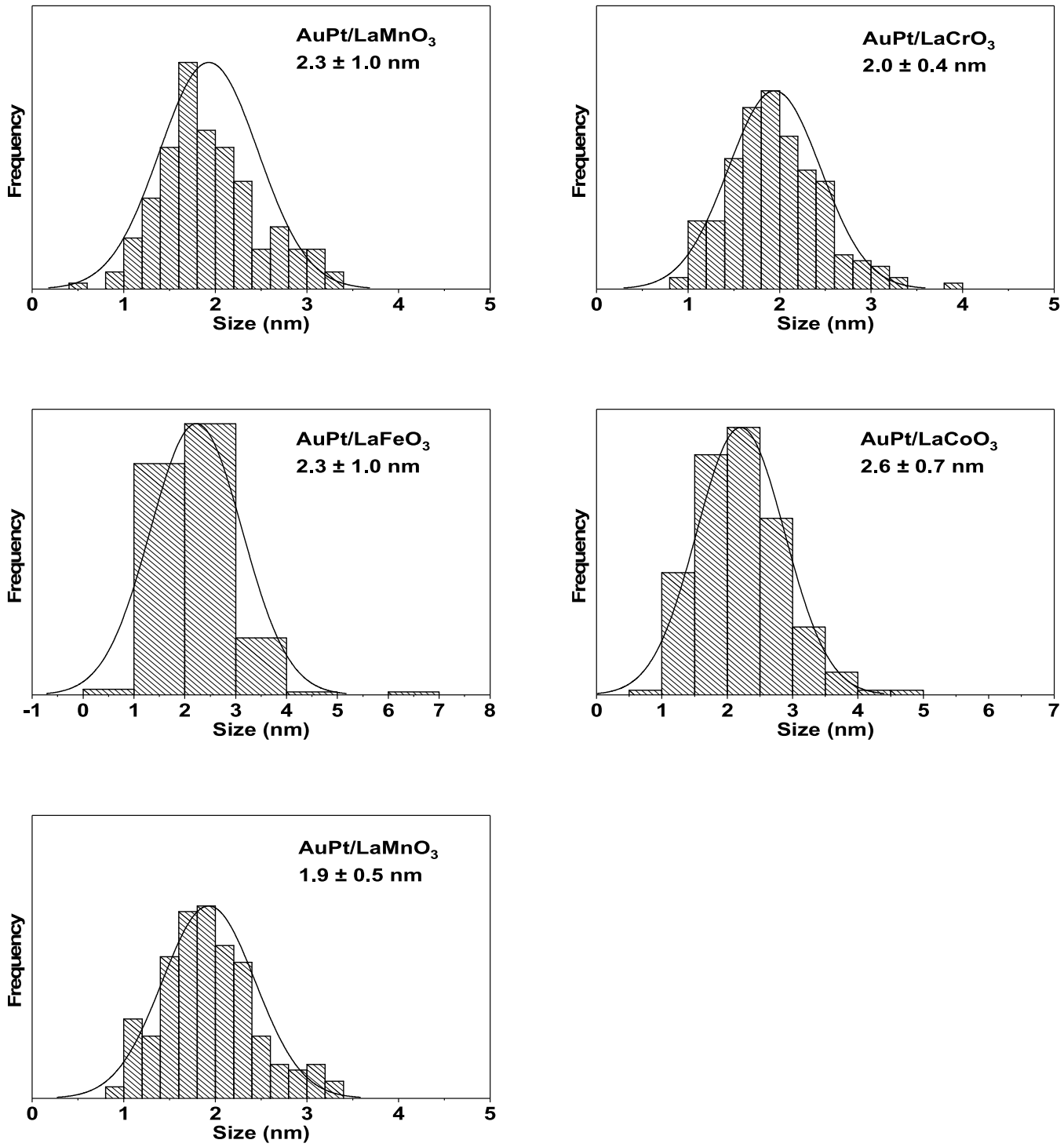

Fig. 4. Particle size distribution histograms of AuPt supported on the different SBA-15 assisted $LaBO_3$ perovskites.

small nanoparticles which is dependent on both the nature of the oxide support and the size of the nanoparticles [29]. The spectra shows the platinum is in an oxidised form with characteristic binding energies of PtO_2 and PtO observed and only small amounts of Pt^0 detected in some of the catalysts. As in the gold spectra, the binding energies are dependent on the nanparticle support interaction [30].

Table 3 shows the bulk and surface Au/Pt atomic ratios determined by MP-AES and XPS respectively. Although the bulk ratios were similar to the target values for all the catalysts, there is a range of surface compositions for the different supports detected by XPS. These changes can be attributed to composition of the metal nanoparticles, monometallic nanoparticles, a change in the composition of the alloy nanoparticles or the formation of core-shell structures dependent on the potential interactions with the various B site cations [31]. Sol-immobilisation is also known to produce both core-shell and random alloys of AuPt nanoparticles, in which the possible morphologies are well represented by the observed XPS metal ratios. Au/Pt ratios close to 1, suggest random alloys, whereas ratios lower than 0.75 are indicative of Au core, Pt shell nanaomparticles [32]. In this study the XPS ratios are not definitive, particularly as some of the ratios are greater than 1. STEM analysis can be used to determine the structure of bimetallic nanoparticles, although this is difficult for AuPt nanoparticles due to the

Table 3
Au and Pt bulk and surface composition for $AuPt/LaBO_3$ catalysts analysed by MP-AES and XPS.

Catalyst	Bulk Au/Pt ratio[a]	Surface Au/Pt ratio[b]
$LaCrO_3$	0.50 (Au), 0.50 (Pt)	1.0
$LaMnO_3$	0.47 (Au), 0.46 (Pt)	1.1
$LaFeO_3$	0.54 (Au), 0.46(Pt)	1.4
$LaCoO_3$	0.55 (Au), 0.50 (Pt)	0.8
$LaNiO_3$	0.50 (Au), 0.50(Pt)	1.5

[a]Bulk Au/Pt ratio from MP-AES
[b]Surface atomic ratio from XPS

similar atomic numbers and weights.

Catalyst testing

Having synthesised that series of perovskite supported AuPt catalysts, they were evaluated as catalysts for the oxidation of glycerol in a glass reactor at 100 °C under 3 bar O_2. The reactions were carried out in the presence of base, using 0.3 M aqueous solution of glycerol with a NaOH:glycerol ratio of 4:1 and a glycerol:catalyst ratio of 1000:1.

Initial experiments investigated the perovskite supports which were found to give ≤ 5 % conversion under these conditions, demonstrating their activity was low in the absence of the metal nanoparticles (Figure S3). The advantage of the relatively high surface area of perovskite supports obtained through utilising the hard templating method using SBA-15 enabled the deposition of small uniform Au and Pt nanoparticles on to the surface of each of the supports with high dispersions. However, the choice of these high area supports was also due to their properties influencing the selectivity of the catalysts and the high surface area also provides a higher number of the functional active sites to assist in the reaction. When the $AuPt/LaBO_3$ catalysts were tested in the glycerol oxidation reaction the conversion was much higher than the supports alone (Fig. 5).

The conversions and turnover frequencies (TOF) for the catalysts (Table 4) are slightly higher than those observed by Hutchings and coworkers under the same conditions [25], illustrating the benefits of the higher surface area perovskite supports.

Although the conversion and TOFs varied for the different catalysts, this is due to the support material properties rather than the metal nanoparticles as the sol immobilisation method gave very similar metal particles independent of the support.

The selectivities to different products were also dependent on the support material (Table 4, Fig. 6). In previous studies, perovskite supports were found to be selective for one of two pathways to either lactic acid *via* a dehydration pathway or a combination of glyceric acid and tartronic acid *via* an oxidative pathway that are summarised in Scheme 1.

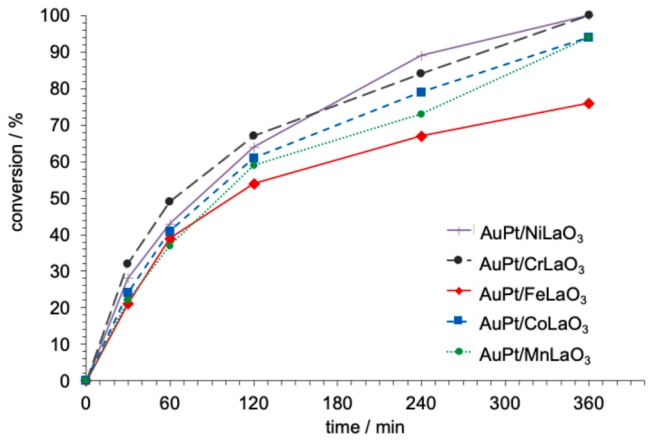

Fig. 5. The conversion of glycerol with $AuPt/LaBO_3$ catalysts. Reaction conditions: glycerol (0.3 M), NaOH: substrate ratio (4:1), O_2 (3 bar), substrate: metal ratio = 1000, 100 °C.

Table 4
Glycerol oxidation over the $AuPt/LaBO_3$ catalysts.[a].

B-site Element	Time (h)	TOF (h^{-1})[b]	Selectivity (%)[c]				CMB[d] (%)
			GA	TA	LA	C-C sc	
Cr	0.5	750	9	4	79	8	96
	1		7	2	81	10	93
	2		7	3	80	10	87
	4		8	2	82	8	82
	6		7	1	82	10	81
Mn	0.5	520	61	5	15	19	100
	1		63	7	15	15	96
	2		65	9	14	12	98
	4		67	11	12	10	89
	6		70	14	10	6	83
Fe	0.5	490	5	31	41	23	99
	1		8	24	42	26	91
	2		5	21	47	27	89
	4		3	19	49	29	84
	6		2	12	55	31	79
Co	0.5	560	61	4	14	21	98
	1		62	3	15	20	99
	2		58	3	17	22	92
	4		52	4	21	23	87
	6		42	4	22	32	84
Ni	0.5	660	45	2	32	21	100
	1		43	3	35	19	96
	2		41	3	39	17	86
	4		39	4	45	12	81
	6		35	6	51	8	79

[a] Reaction conditions: glycerol (0.3 M), NaOH: substrate ratio (4:1), O_2 (3 bar), substrate:metal ratio = 1000, 100 °C.
[b] TOF calculated at 30 min, moles of glycerol converted/moles of metal per h.
[c] Key: GA = glyceric acid, TA = tartronic acid, C–C sc = C_1 and C_2 products, and LA = lactic acid.
[d] Carbon mass balance.

The $AuPt/LaMnO_3$ catalyst was found to favour the production of C_3 products, with a high selectivity to glyceric acid over a period of 6 hours and a relatively low selectivity to the potential C-C scission products (oxalic acid, glycolic acid, formic acid, and CO_2) in line with previous studies. The $AuPt/LaCoO_3$ and $AuPt/LaNiO_3$ catalysts also showed good oxidation performance with high yields of glyceric acid although this was accompanied by a relatively high selectivity to lactic acid, indicating these catalysts contained active sites that could convert glycerol *via* both the dehydration and oxidation routes. $AuPt/LaCrO_3$ was very selective to lactic acid (~80 %) for the time studied and very little oxidation or C-C scission products.

It has been reported that, under these conditions, with the use of AuPt nanoparticles supported on CeO_2 and TiO_2 produce up to 80 % of lactic acid [8,34], which suggests the $LaCrO_3$ support has similar properties. However, at lower reaction temperatures (60 °C) and substrate:base ratios (2:1) have been shown to favour the production of glyceric acid with a selectivity of around 80 %, which is similar to results found here for the $LaMnO_3$ supported catalyst. Above 80 °C with a higher base concentration, the selectivity to LA has been found to dominate with TiO_2 as the support material. However, Tsuji *et al.* reported that Pt/hydrotalcite (HT) catalysts, under similar conditions in the absence of base, achieved 55 % glycerol conversion with high selectivity to GA. The authors noted that dehydration route was completely hindered by these catalysts and ascribed this to the basic nature of the support [35].

In the study by Hutchings and coworkers, selectivity to tartronic acid was generally low compared to glyceric acid for all catalysts [25]. However, for the best oxidation catalysts at high conversion (after 24 h), the tartronic acid increased leading to the conclusion that it was a product of sequential oxidation of glyceric acid. In our study the

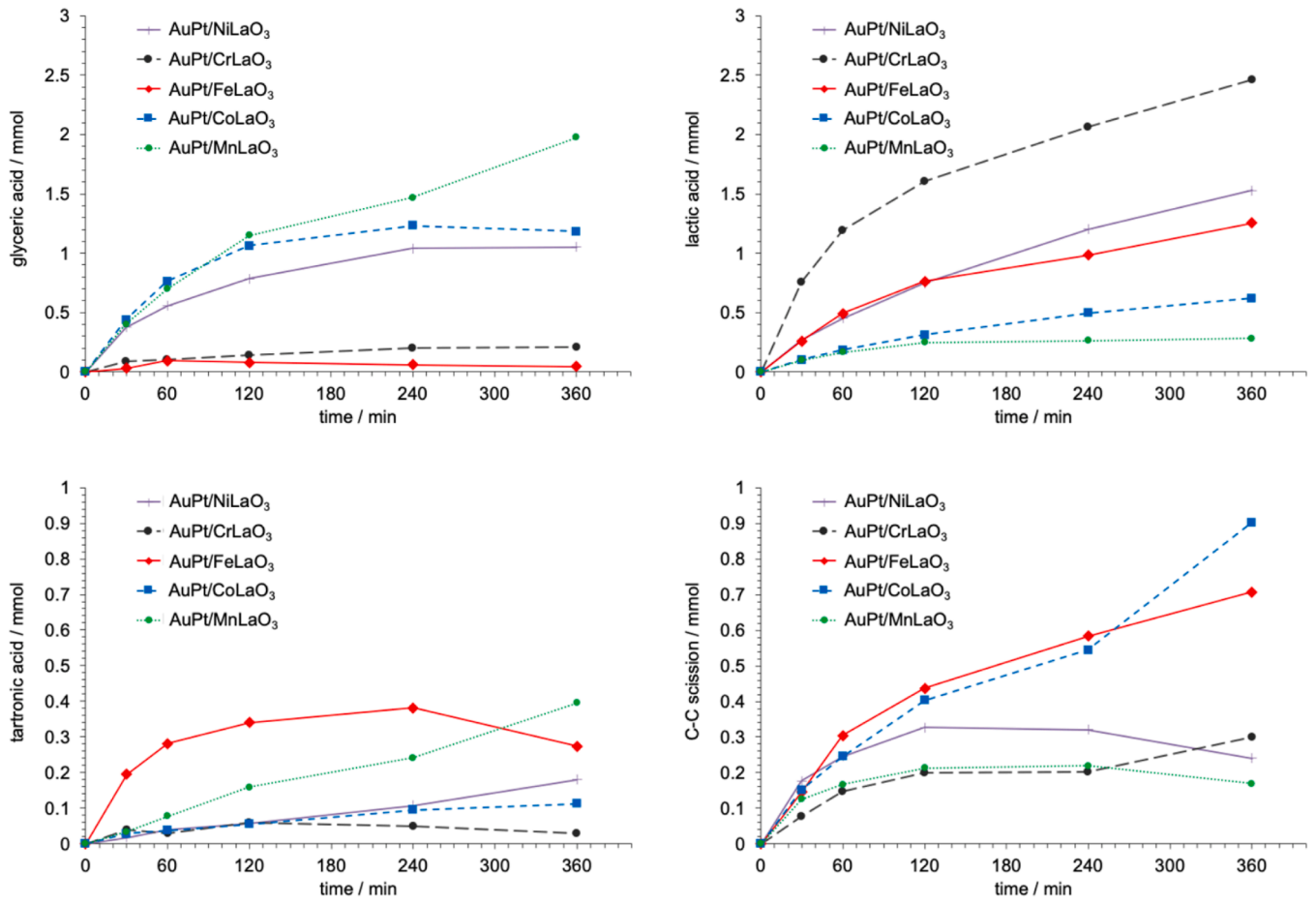

Fig. 6. Time-on-line plot of the moles of products produced during the glycerol oxidation reaction using the AuPt/$LaBO_3$ catalysts: (a) glyceric acid selectivity; (b) lactic acid selectivity; (c) tartronic acid selectivity; and (d) C–C scission selectivity. Reaction conditions: glycerol (0.3 M), NaOH: substrate ratio (4:1), O_2 (3 bar), substrate:metal ratio = 1000, 100 °C.

AuPt/$LaFeO_3$ catalysts gave extremely high tartronic acid selectivity with very little glyceric acid, despite having the lowest conversion of all the perovskite supported catalysts tested. This catalyst also gave a fairly high selectivity to lactic acid, indicating it was not a particularly good oxidation catalyst which does not fit with the sequential oxidation hypothesis. To investigate this discrepancy and to try and understand the mechanism over the different catalysts the number of moles of products produced were plotted to determine how these changed with time-on-line (Fig. 6).

From Fig. 6 it is clear that the selectivities to the different pathways are changing with time-on-line for several of the catalysts. The best performing oxidation catalyst, AuPt/$LaMnO_3$, produces the highest amount of glyceric acid and after 6 hours, the highest amount of tartronic acid. However, the rate of production and ratio of these two products remains similar over the course of the reaction, suggesting that the formation of glyceric acid and its sequential oxidation to tartonic acid occurs at a similar rate. The production of lactic acid is low and after the first hour the dehydration sites appear to switch off and no further lactic acid is produced. Similarly, The C-C scission products remain at a constant rate over the course of the reaction after the first hour.

For the other catalalysts, AuPt/$LaCrO_3$, AuPt/$LaFeO_3$, AuPt/$LaCoO_3$, AuPt/$LaNiO_3$, no products from the oxidative route are produced after 2 hours, indicating that these sites are deactivated during the reaction, while the lactic acid continues to increase at a steady rate during the reaction, showing that the dehydration pathway remains active.

The AuPt/$LaFeO_3$ catalyst shows particularly interesting behaviour. The selectivity to tartronic acid is the highest observed for these catalysts and this is unusual as it is typically only formed for longer time-on-line with good oxidation catalysts from the sequential oxidation of glyceric acid once the glycerol has all been converted. Not only was AuPt/$LaFeO_3$ found to give the lowest conversion, it also produced very little glyceric acid suggesting the sequential oxidation process is favoured over this catalyst. It is also interesting that the major reaction product was lactic acid, indicating this catalyst must have a balance of sites responsible for the dehydration and oxidation pathways which suggests it has a lower concentration of oxidation sites, but these are very active. This was the only perovskite that was found to have a phase segregated B site oxide present by XRD (Fe_2O_3), so this may be the cause of the very active oxidation sites. However, an AuPt/Fe_2O_3 catalyst has been previously tested under similar conditions and found to produce a high amount of C-C scission products, so this previous result and the low amounts of Fe_2O_3 suggest this is unlikely to be responsible for the high amounts of tartronic acid. For AuPt/$LaFeO_3$ and AuPt/$LaCoO_3$, the C-C scission products increase throughout the reaction. These products have been suggested to form over single oxide impurities in the perovskites suggesting that the supports are unstable under the reaction conditions. For all catalysts the carbon mass balance reduced during the course of the reaction (Table 3), which is attributed to humins that are often found to be secondary products in this and similar reactions.

The changes in product distribution during the reaction for all the catalysts are a clear indication that the perovskite materials are evolving over the course of the reaction. Kondrat and coworkers have investigated lanthanum based perovskites as supports in the aqueous phase reforming of glycerol [36–38]. Although these experiments are carried out under reducing rather than oxidising conditions, detailed

characterisation studies showed that perovskites typically phase separate in solution to give single oxides as well as leaching of some metals into solution. Although these changes often resulted in no loss in performance for reforming, for such a structure sensitive reaction like glycerol oxidation, where there are competing pathways to different product families, these changes could impact on the product distribution.

Conclusions

The use of a hard templating route with SBA-15 was found to give high surface area perovskites that could be used as catalyst supports for AuPt nanoparticles, resulting in a series of $LaBO_3$ supports (where B = Cr, Mn, Fe, Co or Ni) with surface areas of 70–160 $m^2\,g^{-1}$. Although this study used 1 wt% of metal to compare results to previous studies, it offers a potential route to increasing the metal loading further to increase space time yields of products.

When the AuPt/$LaBO_3$ catalysts were tested for glycerol oxidation the product distributions could be tuned by substituting different transition metals in the B site. In line with previous studies, AuPt/$LaMnO_3$ and AuPt/$LaCoO_3$ gave the highest yield of oxidation products (glyceric acid with small amounts of tartronic acid), whereas AuPt/$LaCrO_3$ gave the highest yield of lactic acid.

AuPt/$LaNiO_3$ was found to give a reasonable selectivity to both glyceric acid and lactic acid, showing it had active sites that could direct the conversion of glycerol down both the oxidation and dehydration pathways. Over the course of the reaction (6 h) the selectivity switched from glyceric acid being the major product initially to lactic acid being the major product for reaction times longer than 2 h.

This switch in selectivity led us to investigate the product distributions in more detail and found that all the catalysts had changes in performance with time-on-line. For all catalysts except AuPt/$LaMnO_3$ the yield of oxidation products stopped after a couple of hours, while all catalysts except AuPt/$LaMnO_3$ continued to produce lactic acid over the whole reaction. This suggests the perovskite supported catalysts are not stable over the course of the reaction, supporting the findings of Kondrat and coworkers for perovskite supported reforming catalysts.

The most interesting behaviour was found for the AuPt/$LaFeO_3$ catalyst that gave a high initial selectivity to tartronic acid. Typically, tartronic acid is only seen in high quantities when glyceric acid is sequentially oxidised after long reaction times. However, over the AuPt/$LaFeO_3$ catalyst tartronic acid is produced initially, with very low amounts of glyceric acid, indicating that the oxidation of glyceric acid is very fast over this catalyst or tartronic acid is being produced *via* a different route. However further studies are needed to elucidate the mechanism fully.

CRediT authorship contribution statement

Hamza S. Rabiu: Writing – original draft, Validation, Methodology, Investigation, Data curation, Conceptualization. **James S. Hayward:** Supervision, Methodology, Investigation, Conceptualization. **Jonathan K. Bartley:** Writing – original draft, Validation, Supervision, Methodology, Formal analysis, Conceptualization.

Declaration of competing interest

The authors declare the following financial interests/personal relationships which may be considered as potential competing interests:

Hamza Rabiu reports financial support was provided by Petroleum Technology Development Fund. If there are other authors, they declare that they have no known competing financial interests or personal relationships that could have appeared to influence the work reported in this paper.

Acknowledgements

HSR thanks The Petroleum Technology Development Fund for an overseas postgraduate scholarship.

Supplementary materials

Supplementary material associated with this article can be found, in the online version, at doi:10.1016/j.mcat.2024.114750.

Data availability

The datasets generated during the current study are available free of charge through the Cardiff University Research Portal https://doi.org/10.12035/cardiff.26495962.

References

[1] A. Galadima, O. Muraza, Biodiesel production from algae by using heterogeneous catalysts: a critical review, Energy 78 (2014) 72–83, https://doi.org/10.1016/j.energy.2014.06.018.
[2] M.G. Kulkarni, R. Gopinath, L.C. Meher, A.K. Dalai, Solid acid catalyzed biodiesel production by simultaneous esterification and transesterification, Green. Chem. 8 (2006) 1056–1062, https://doi.org/10.1039/B605713F.
[3] H. Sani, U. Gaya, Methanolysis of Gmelina Seed Oil to Biodiesel with KNO_3 Activated MgO-ZnO Composite Catalyst, J. Turkish Chem. Soc. Sect. A Chem. 6 (2019) 335–348, https://doi.org/10.18596/jotcsa.491458.
[4] R. Garcia, M. Besson, P. Gallezot, Chemoselective catalytic oxidation of glycerol with air on platinum metals, Appl. Catal. A Gen. 127 (1995) 165–176, https://doi.org/10.1016/0926-860X(95)00048-8.
[5] A. Villa, N. Dimitratos, C.E. Chan-Thaw, C. Hammond, L. Prati, G.J. Hutchings, Glycerol oxidation using gold-containing catalysts, Acc. Chem. Res. 48 (2015) 1403–1412, https://doi.org/10.1021/ar500426g.
[6] N. Dimitratos, J.A. Lopez-Sanchez, D. Lennon, F. Porta, L. Prati, A. Villa, Effect of particle size on monometallic and bimetallic (Au,Pd)/C on the liquid phase oxidation of glycerol, Catal. Lett. 108 (2006) 147–153, https://doi.org/10.1007/s10562-006-0036-8.
[7] S. Gil, M. Marchena, L. Sánchez-Silva, A. Romero, P. Sáncheza, J.L. Valverde, Effect of the operation conditions on the selective oxidation of glycerol with catalysts based on Au supported on carbonaceous materials, Chem. Eng. J. 178 (2011) 423–435, https://doi.org/10.1016/j.cej.2011.10.048.
[8] M. Douthwaite, N. Powell, A. Taylor, G. Ford, J.M. López, B. Solsona, N. Yang, O. Sanahuja-Parejo, Q. He, D.J. Morgan, T. Garcia, S.H. Taylor, Glycerol selective oxidation to lactic acid over aupt nanoparticles; enhancing reaction selectivity and understanding by support modification, ChemCatChem. (2020) 3097–3107, https://doi.org/10.1002/cctc.202000026.
[9] (2024). https://creativecommons.org/share-your-work/cclicenses/.
[10] L. Prati, M. Rossi, Chemoselective catalytic oxidation of polyols with dioxygen on gold supported catalysts, Stud. Surf. Sci. Catal. 110 (1997) 509–515, https://doi.org/10.1016/S0167-2991(97)81012-9.
[11] N. Dimitratos, J.A. Lopez-Sanchez, J.M. Anthonykutty, G. Brett, A.F. Carley, R. C. Tiruvalam, A.A. Herzing, C.J. Kiely, D.W. Knight, G.J. Hutchings, Oxidation of glycerol using gold–palladium alloy-supported nanocrystals, Phys. Chem. Chem. Phys. 11 (2009) 4952–4961, https://doi.org/10.1039/b904317a.
[12] W.C. Ketchie, M. Murayama, R.J. Davis, Selective oxidation of glycerol over carbon-supported AuPd catalysts, J. Catal. 250 (2007) 264–273, https://doi.org/10.1016/j.jcat.2007.06.011.
[13] M.S. Ide, R.J. Davis, The important role of hydroxyl on oxidation catalysis by gold nanoparticles, Acc. Chem. Res. 47 (2014) 825–833, https://doi.org/10.1021/ar4001907.
[14] B.N. Zope, D.D. Hibbitts, M. Neurock, R.J. Davis, Reactivity of the gold/water interface during selective oxidation catalysis, Science (1979) 330 (2010) 74–78, https://doi.org/10.1126/science.1195055.
[15] W.C. Ketchie, M. Murayama, R.J. Davis, Promotional effect of hydroxyl on the aqueous phase oxidation of carbon monoxide and glycerol over supported Au catalysts, Top. Catal. 44 (2007) 307–317, https://doi.org/10.1007/s11244-007-0304-x.
[16] L. Prati, A. Villa, C.E. Chan-Thaw, R. Arrigo, D. Wang, D.S. Su, Gold catalyzed liquid phase oxidation of alcohol: the issue of selectivity, Faraday Discuss. 152 (2011) 353–365, https://doi.org/10.1039/c1fd00016k.
[17] A. Namdeo, S.M. Mahajani, A.K. Suresh, Palladium catalysed oxidation of glycerol - effect of catalyst support, J. Mol. Catal. A, Chem. 421 (2016) 45–56, https://doi.org/10.1016/j.molcata.2016.05.008.
[18] C. Xu, Y. Du, C. Li, J. Yang, G. Yang, Insight into effect of acid/base nature of supports on selectivity of glycerol oxidation over supported Au-Pt bimetallic catalysts, Appl. Catal. B, Environ. 164 (2015) 334–343, https://doi.org/10.1016/j.apcatb.2014.09.048.
[19] B. Katryniok, H. Kimura, E. Skrzyńska, J.-S. Girardon, P. Fongarland, M. Capron, R. Ducoulombier, N. Mimura, S. Paul, F. Dumeignil, Selective catalytic oxidation of glycerol: perspectives for high value chemicals, Green. Chem. 13 (2011) 1960–1979, https://doi.org/10.1039/C1GC15320J.

[20] S. Liu, K. Sun, B. Xu, Specific selectivity of au-catalyzed oxidation of glycerol and other c_3-polyols in water without the presence of a base, ACS Catal. 4 (2014) 2226–2230, https://doi.org/10.1021/cs5005568.
[21] A. Villa, S. Campisi, K.M.H. Mohammed, N. Dimitratos, F. Vindigni, M. Manzoli, W. Jones, M. Bowker, G.J. Hutchings, L. Prati, Tailoring the selectivity of glycerol oxidation by tuning the acid–base properties of Au catalysts, Catal. Sci. Technol. 2 (2015) 1126–1132, https://doi.org/10.1039/c4cy01246a.
[22] N.F. Atta, A. Galal, E.H. El-Ads, Perovskite nanomaterials – synthesis, characterization, and applications, in: L. Pan, G. Zhu (Eds.), Perovskite Materials - Synthesis, Characterisation, Properties, and Applications, Intech, 2016, https://doi.org/10.5772/60469.
[23] P.R.N. Silva, A.B. Soares, Lanthanum based high surface area perovskite-type oxide and application in CO and propane combustion, Eclet. Quim. 34 (2009) 31–38, https://doi.org/10.26850/1678-4618eqj.v34.1.2009.p31-38.
[24] H. Zhu, P. Zhang, S. Dai, Recent advances of lanthanum-based perovskite oxides for catalysis, ACS Catal. 5 (2015) 6370–6385, https://doi.org/10.1021/acscatal.5b01667.
[25] C.D. Evans, S.A. Kondrat, P.J. Smith, T.D. Manning, P.J. Miedziak, G.L. Brett, R. D. Armstrong, J.K. Bartley, S.H. Taylor, M.J. Rosseinsky, G.J. Hutchings, Faraday Discuss. 188 (2016) 427–450, https://doi.org/10.1039/c5fd00187k.
[26] H. Deng, L. Lin, S Liu, Catalysis of cu-doped co-based perovskite-type oxide in wet oxidation of lignin to produce aromatic aldehydes, Energy Fuels. 24 (2010) 97–4802, https://doi.org/10.1021/ef100768e.
[27] X. Huang, G. Zhao, G. Wang, J.T.S. Irvine, Synthesis and applications of nanoporous perovskite metal oxides, Chem. Sci. 9 (2018) 3623–3637, https://doi.org/10.1039/C7SC03920D.
[28] S. Afzal, X. Quan, J. Zhang, High surface area mesoporous nanocast $LaMO_3$ (M = Mn, Fe) perovskites for efficient catalytic ozonation and an insight into probable catalytic mechanism, Appl. Catal. B Environ. 206 (2017) 692–703, https://doi.org/10.1016/j.apcatb.2017.01.072.
[29] J. Radnik, C. Mohr, Claus On the origin of binding energy shifts of core levels of supported gold nanoparticles and dependence of pretreatment and material synthesis, Phys. Chem. Chem. Phys. 5 (2003) 172–177, https://doi.org/10.1039/B207290D.
[30] L.K. Ono, B. Yuan, H. Heinrich, B.Roldan Cuenya, Formation and thermal stability of platinum oxides on size-selected platinum nanoparticles: support effects, J. Phys. Chem. C 114 (2010) 22119–22133, https://doi.org/10.1021/jp1086703.
[31] N. Dimitratos, J.A. Lopez-Sanchez, D. Morgan, A.F. Carley, R. Tiruvalam, C. J. Kiely, D. Bethell, G.J. Hutchings, Solvent-free oxidation of benzyl alcohol using Au – Pd catalysts prepared by sol immobilisation, Phys. Chem. Chem. Phys. 11 (2009) 5142–5153, https://doi.org/10.1039/b900151b.
[32] S. Carrettin, P. McMorn, P. Johnston, K. Griffin, C.J. Kiely, G.J. Hutchings, Oxidation of glycerol using supported Pt, Pd and Au catalysts, Phys. Chem. Chem. Phys. 5 (2003) 1329–1336, https://doi.org/10.1039/b212047j.
[33] X. Huang, O. Akdim, M. Douthwaite, K. Wang, L. Zhao, R.J. Lewis, S. Pattisson, I. T. Daniel, P.J. Miedziak, G. Shaw, D.J. Morgan, S.M. Althahban, T.E. Davies, Q. He, F. Wang, J. Fu, D. Bethell, S. McIntosh, C.J. Kiely, G.J. Hutchings, Au-Pd separation enhances bimetallic catalysis of alcohol oxidation, Nature 603 (2022) 271–275, https://doi.org/10.1038/s41586-022-04397-7.
[34] P. Lakshmanan, P.P. Upare, N.-T. Le, Y.K. Hwang, D.W. Hwang, U.-H. Lee, J.-S. Chang H.R.Kim, Facile synthesis of CeO_2-supported gold nanoparticle catalysts for selective oxidation of glycerol into lactic acid, Appl. Catal. A, Gen. 468 (2013) 260–268, https://doi.org/10.1016/j.apcata.2013.08.048.
[35] A. Tsuji, K.T.V. Rao, S. Nishimura, A. Takagaki, K. Ebitani, Selective oxidation of glycerol by using a hydrotalcite-supported platinum catalyst under atmospheric oxygen pressure in water, ChemSusChem. 4 (2011) 542–548, https://doi.org/10.1002/cssc.201000359.
[36] D.R. Inns, A.J. Mayer, V. Skukauskas, T.E. Davies, J. Callison, S.A. Kondrat, Evaluating the activity and stability of perovskite LaMO 3 -based Pt catalysts in the aqueous phase reforming of glycerol, Top. Catal. 64 (2021) 992–1009, https://doi.org/10.1007/s11244-021-01449-6.
[37] D.R. Inns, X. Pei, Z. Zhou, D.J.M. Irving, S.A. Kondrat, The influence of phase purity on the stability of $Pt/LaAlO_3$ catalysts in the aqueous phase reforming of glycerol, Mater. Today Chem. 26 (2022) 101230, https://doi.org/10.1016/j.mtchem.2022.101230.
[38] P. Nagy, D.R. Inns, S.A. Kondrat, J.L. Wagner, The effect of flow conditions on the activity and stability of $Pt/LaAlO_3$ perovskite catalyst during aqueous phase reforming of glycerol, Chem. Eng. J. 483 (2024) 149274, https://doi.org/10.1016/j.cej.2024.149274.